Journal of Applied Mathematics and Physics, 2025, 13(3), 709-728
https://www.scirp.org/journal/jamp
ISSN Online: 2327-4379
ISSN Print: 2327-4352

Heat and Mass Transfer in Unsteady Magneto-Hydrodynamic Nanofuid Flow through a Divergent Conduit with Chemical Reaction and Radiation

Valarie Nyakerario Nyabuti*, Edward Richard Onyango, Phineas Roy Kiogora

Department of Pure and Applied Mathematics, Jomo Kenyatta University of Agriculture and Technology, Nairobi, Kenya
Email: *valarienyakerario@gmail.com, edward.onyango@jkuat.ac.ke, prkiogora@jkuat.ac.ke

How to cite this paper: Nyabuti, V.N., Onyango, E.R. and Kiogora, P.R. (2025) Heat and Mass Transfer in Unsteady Magneto-Hydrodynamic Nanofuid Flow through a Divergent Conduit with Chemical Reaction and Radiation. *Journal of Applied Mathematics and Physics*, **13**, 709-728.
https://doi.org/10.4236/jamp.2025.133039

Received: January 13, 2025
Accepted: March 16, 2025
Published: March 19, 2025

Abstract

Heat and mass transfer in unsteady Magneto-Hydrodynamic (MHD) nanofluid (Silver-water) flow through a divergent conduit with chemical reaction and radiation has been investigated. The study aimed to determine the distribution of energy and nanoparticles in the system. The governing non-linear partial differential equations are transformed into non-linear ordinary differential equations using similarity transforms and numerically solved using the spectral collocation method. The resultant system of equations has been implemented in MATLAB to generate graphical results. The rate of heat transfer increased with an increase in the Eckert number and Joule heating parameter and decreased with increasing radiation parameter whereas the mass transfer rate increased with an increase in the Schmidt number, Soret number, and Chemical reaction parameter. These research findings would be useful to engineers and researchers in designing optimal heat exchanger systems to maximize heat and mass transfers in the geothermal industry.

Keywords

Heat and Mass Transfer, MHD, Nanofluid, Divergent Conduit

1. Introduction

Heat exchangers are crucial for facilitating heat transfer processes in various industrial settings including the geothermal sector where efficient heat transfer is crucial for extracting energy from geothermal sources. Optimizing heat transfer within these heat exchanger systems is essential for maximizing energy production.

Recent advancements in nanotechnology have introduced nanofluids, which are suspensions of nanoparticles (Silver) in a base fluid (water) as promising heat transfer fluids due to their enhanced thermal properties. Haroun *et al.* [1] examined nanoparticles and found that they enhanced heat transfer in fluids. The utilization of nanofluids in heat exchanger systems has the potential to significantly improve thermal performance. Heat transfer in nanofluids for potential use in engineering and energy systems was researched by Phelan *et al.* [2].

Magneto-hydrodynamics (MHD) involves electrically conducting fluids interacting with a magnetic field as first researched by Alfven *et al.* [3]. The presence of a magnetic field can significantly influence the flow and heat transfer characteristics of nanofluids. The Lorentz force generated acts on the electrically conducting fluid, potentially altering the flow patterns and heat transfer rates.

The effect of heat and mass transfer on unsteady MHD nanofluid flow through a convergent-divergent channel was investigated by Habiyaremye *et al.* [4]. They used the collocation method to solve the system of first-order ordinary differential equations and implemented the bvp4c function in MATLAB software. They found that the velocity and temperature of the nanofluid increment with the increase in the heat generation parameter for both the convergent and divergent channels whereas the concentration of the nanofluid decreased with an increase in the heat generation parameter.

Heat and mass transfer in a viscous unsteady MHD nanofluid flow through a channel with porous walls and medium in the presence of metallic nanoparticles was analyzed by Zubair *et al.* [5]. They observed that the heat transfer rate increased with the increase of Reynolds number while the mass transfer rate decreased with the increase of Reynolds number. Govardhan *et al.* [6] numerically analyzed the viscous dissipation effect of MHD nanofluid flow over a stretching surface with heat and mass transfer. The concentration profile augmented with the gradual increase of the thermophoresis parameter.

Chemical reactions occurring within the nanofluid and thermal radiation can further impact heat transfer by generating or absorbing thermal energy. These influence the fluid thermal properties and mass transfer rates. The effects of chemical reaction on hydromagnetic natural convection flow of Casson nanofluid induced due to non-linearly stretching sheet immersed in a porous medium under the influence of thermal radiation and convective boundary condition was investigated by Ullah *et al.* [7]. They used similarity transformations to convert the governing non-linear partial differential equations into ordinary differential equations and solved numerically using the Keller Box method. They found out that the presence of nanoparticles effectively promotes the heat transfer mechanism in the base fluid.

Heat and mass transfer in unsteady MHD Casson fluid flow with convective boundary conditions was researched by Pushpalatha *et al.* [8]. They analytically solved the governing equations using the perturbation technique. They observed that the thermal diffusion parameter tends to enhance the velocity and concentra-

tion profiles and that the conviction parameter enhanced the heat transfer rate. They also noted that increasing the values of the Suction parameter enhanced heat and mass transfer rate.

A research on heat and mass transfer in nanofluid flows with magneto-hydrodynamic conditions over cone and wedge was conducted by Sujatha *et al.* [9]. The transformed governing equations were solved using the shooting technique based on the RK fourth-order method. Their research was significant for designing heat exchangers.

The Jeffrey-Hamel flow of a viscous incompressible fluid that conducts electricity via a diverging conduit in the presence of an inclined variable magnetic field with heat and mass transfer was studied by Onyango *et al.* [10]. They noted that the temperature increased with an increase in Eckert number, Hartmann number, wedge angle, and Grashof Temperature number while the concentration of the fluid increased with an increase in the wedge angle and unsteadiness parameter.

A study of heat and mass transfer on the MHD flow of nanoparticles was conducted by Mohyud-Din *et al.* [11] using Buongiorno's model. Similarity transforms were used to reduce PDEs into nonlinear ODEs and numerically solved using the Runge-Kutta-Fehlberg method coupled with the shooting procedure. Nyariki *et al.* [12] researched heat and mass transfer in a two-phase stratified turbulent flow in a geothermal pipe with chemical reaction. They observed that the heat transfer rate increased with an increase in the angle of inclination and Eckert number while the mass transfer rate increased with an increase in chemical reaction parameter and Reynolds number.

Unsteady MHD nanofluid flow through a diverging conduit with chemical reaction and radiation was researched by Nyabuti *et al.* [13]. They noted that increasing the radiation parameter decreased the temperature of the nanofluid while increasing the Chemical reaction parameter and Soret number increased the concentration of the nanofluid.

Numerical simulation of heat and mass transfer in magnetic nanofluid flow by a rotating disk with variable fluid properties was examined by Sharma *et al.* [14]. They considered the ferrohydrodynamic flow of magnetic nanofluid caused by a rotating disk with temperature-dependent thermal conductivity and geothermal viscosity. They observed that increasing the Prandtl number enhanced the heat transfer rate while the concentration decreased with larger values of the rotation parameter.

A study on the influence of chemical reaction and non-linear thermal radiation on MHD three-dimensional heat and mass transfer boundary layer flow over a stretching sheet filled with water-based alumina nanofluid was conducted by Sudarsan *et al.* [15]. They noticed that the heat transfer rate increased with higher values of the nanoparticle volume fraction parameter while the heat transfer rate decreased as the values of the suction parameter increased.

Little attention has been given to heat and mass transfer rates in MHD nanofluid flows when chemical reactions and radiation are combined. This pre-

sent study investigates heat and mass transfer in unsteady MHD nanofluid flow through a divergent conduit, incorporating chemical reaction and radiation.

2. Mathematical Formulation

A two-dimensional MHD nanofluid flow through a diverging conduit is illustrated in Figure 1. The flow is assumed to be unsteady, incompressible, and of the Power Law non-linear viscosity model. The nanofluid is non-Newtonian in nature with chemical reactions considered to be of first-order and radiation effects being in a steady state. The fluid flow is assumed to be purely radial with a constant magnetic field. The cylindrical polar coordinate system is (r,θ,z) with the angle $|\alpha|>0$ describing the diverging section, and the velocity of the nanofluid being:

$$\boldsymbol{v}=\boldsymbol{v}(r,\theta,t) \tag{1}$$

The velocity of the nanofluid is maximum at the center and reduces as it approaches the walls of the conduit.

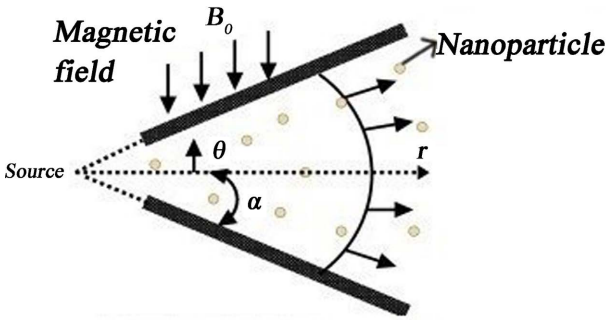

Figure 1. Flow geometry.

From the aforementioned assumptions, the governing equations in cylindrical coordinates are presented as: *Equation of Continuity*

$$\rho_{nf}\left[\frac{1}{r}\frac{\partial\left(ru_r^*\right)}{\partial r}\right]=0 \tag{2}$$

Equation of Conservation of Momentum in radial direction, $\hat{r}$:

$$\begin{aligned}\rho_{nf}\frac{\partial u_r^*}{\partial t}=&-\frac{\partial p}{\partial r}+2\frac{\partial\mu}{\partial r}\frac{\partial u_r^*}{\partial r}+\frac{1}{r^2}\frac{\partial\mu}{\partial\theta}\frac{\partial u_r^*}{\partial\theta}\\&+\mu\left[\frac{1}{r^2}\frac{\partial^2u_r^*}{\partial\theta^2}+2\left(\frac{\partial^2u_r^*}{\partial r^2}+\frac{1}{r}\frac{\partial u_r^*}{\partial r}-\frac{u_r^*}{r^2}\right)\right]\\&-\rho_{nf}u_r^*\frac{\partial u_r^*}{\partial r}-\sigma B_0^2u_r^*\hat{r}\end{aligned} \tag{3}$$

Equation of Conservation of Momentum in θ *-direction,* $\hat{\theta}$:

$$0=-\frac{1}{r}\frac{\partial p}{\partial\theta}+\frac{1}{r}\frac{\partial\mu}{\partial r}\frac{\partial u_r^*}{\partial\theta}+2\frac{u_r^*}{r^2}\frac{\partial\mu}{\partial\theta}+2\frac{\mu}{r^2}\frac{\partial u_r^*}{\partial\theta}+\mu\left[\frac{1}{r}\left(\frac{\partial^2u_r^*}{\partial r\partial\theta}+\frac{1}{r}\frac{\partial u_r^*}{\partial\theta}\right)\right] \tag{4}$$

Equation of Energy

$$\frac{\partial T}{\partial t}+u_r^*\frac{\partial T}{\partial r}=\frac{k_{nf}}{\rho_{nf}C_p}\left[\frac{1}{r}\frac{\partial}{\partial r}\left(r\frac{\partial T}{\partial r}\right)+\frac{1}{r^2}\frac{\partial^2 T}{\partial\theta^2}\right]+\frac{2\mu}{\rho_{nf}C_p}\left[\left(\frac{\partial u_r^*}{\partial r}\right)^2+\left(\frac{u_r^*}{r}\right)^2\right]+\frac{\mu}{\rho_{nf}C_p}\left[\left(\frac{1}{r}\frac{\partial u_r^*}{\partial\theta}\right)^2\right]+\frac{\sigma B_0^2 u_r^{*2}}{\rho_{nf}C_p}-\frac{1}{\rho_{nf}C_p}\frac{\partial}{\partial r}\left(q_{r,rad}\right)-\frac{1}{r\rho_{nf}C_p}\frac{\partial}{\partial\theta}\left(q_{\theta,rad}\right) \tag{5}$$

According to Rosseland's approximation Pantokratoras *et al.* [16] and Dogonchi *et al.* [17], the radiative heat flux for thermal radiation is given by:

$$q_{r,rad}=-\frac{4\sigma^*}{3k_{nf}}\frac{\partial T^4}{\partial r} \tag{6}$$

$$q_{\theta,rad}=-\frac{4\sigma^*}{3k_{nf}}\frac{\partial T^4}{\partial\theta} \tag{7}$$

where σ^* is the Stefan-Boltzmann constant and k_{nf} is the mean absorption coefficient of the nanofluid.

Equation of Concentration

$$\frac{\partial C}{\partial t}+\frac{u_r^*}{r}\frac{\partial(rC)}{\partial r}=D_{nf}\left(\frac{1}{r}\frac{\partial}{\partial r}\left(r\frac{\partial C}{\partial r}\right)+\frac{1}{r^2}\frac{\partial^2 C}{\partial\theta^2}\right)-k_r\left(C-C_\infty\right)+\frac{D_{nf}K_t}{T_\infty}\left(\frac{\partial T}{\partial r}\hat{r}+\frac{1}{r}\frac{\partial T}{\partial\theta}\hat{\theta}\right) \tag{8}$$

2.1. Thermo-Physical Properties

Nanoparticles in nanofluids enhance heat transfer rates by showing temperature differences. Thermo-physical properties such as thermal conductivity, nanoparticle volume fraction, and base fluid material determine the heat transfer behavior of the nanofluid. The following Table 1 displays the thermo-physical properties of Silver-water nanofluid considered in this study.

Table 1. Thermo-physical properties of silver and water.

Nanoparticles	C_p	K	ρ	σ
Water	997.1	4179	0.613	0.06
Silver	10500	235	4291	6.3×10^7

Taking into account the non-Newtonian nature of the nanofluid, the Power Law model was applied due to its shear-thickening behavior that is normally observed in the Silver-Water nanofluids. This property accounts for the varying shear rates at a higher accuracy and accommodates changes in viscosity under varying flow conditions. The power Law Model expressed viscosity as:

$$\mu=\mu_0 g^{n-1}(\theta) \tag{9}$$

with θ being a subset of angle α. This viscosity increases with the shear rate

due to the shear-thickening behavior of the non-Newtonian fluid. The term given for such a fluid is dilatant fluid and for this study, $n>1$. This range n, which reflects the sensitivity of viscosity to the shear rate, is consistent with findings from Mahbubul *et al.* [18], which demonstrated dilatant behavior in silver-water nanofluids at higher shear rates. Sundar *et al.* [19] studied the thermal conductivity and viscosity properties of silver-water nanofluids at similar nanoparticle concentrations and flow conditions. The value of μ_0 was derived based on experimental data reported by Sundar *et al.* [19], where silver-water nanofluids were studied at a nanoparticle volume fraction of 2% and temperatures ranging from 25˚C to 50˚C. The value chosen reflects the base viscosity at a unit shear rate. Therefore:

$$g(\theta)=\theta^c, \tag{10}$$

for $c>1$ where c is an arbitrary constant.

Then Equation (9) becomes:

$$\mu=\mu_0\theta^{c(n-1)} \tag{11}$$

The boundary conditions considered are:
at the center line, $\theta=0$:

$$\begin{aligned} &u_r^*=u_\infty^*, \frac{\partial u_r^*}{\partial\theta}=0, T=T_\infty, \frac{\partial T}{\partial\theta}=0, \\ &C=C_\infty, \frac{\partial C}{\partial\theta}=0 \end{aligned} \tag{12}$$

on the wall, $\theta=\alpha$:

$$\frac{\partial u_r^*}{\partial\theta}=-\gamma u^*(\theta), T=T_\omega, C=C_\omega \tag{13}$$

where u_∞^* is the velocity at the center line, T_∞ and C_∞ are the free stream temperature and concentration respectively, T_ω, C_ω are the temperature and concentration at the wall, α is the wedge angle and $\gamma\geq 0$ is the friction coefficient factor.

2.2. Similarity Transformation

Similarity transformations are used to reduce the governing non-linear Partial Differential Equations (PDEs) 2, 3, 4, 5 and 8 into non-linear Ordinary Differential Equations (ODEs). From Nagler *et al.* [20] and Sattar *et al.* [21], the similarity transformation of velocity is described as:

$$u_r^*(r,\theta,t)=-\frac{Q}{r}\frac{1}{\delta^{m+1}}F(\eta) \tag{14}$$

where Q is the planar volumetric flow rate, m is a constant related to the angle α, δ is the time dependent length scale, and F is the dimensionless fluid velocity. The similarity transformations for temperature and concentration are given by:

$$\frac{\omega(\eta)}{\delta^{m+1}} = \frac{T - T_\omega}{T_\infty - T_\omega} \tag{15}$$

$$\frac{\phi(\eta)}{\delta^{m+1}} = \frac{C - C_\omega}{C_\infty - C_\omega} \tag{16}$$

where $\omega(\eta)$ denotes the dimensionless temperature, $\phi(\eta)$ denotes the dimensionless concentration and η is a dimensionless parameter expressed as:

$$\eta = \frac{\theta}{\alpha} \tag{17}$$

$$\rho_{nf}\left[\frac{1}{r}\frac{\partial\left(ru_r^*\right)}{\partial r}\right] = \rho_{nf}\left[\frac{Q}{r}\frac{1}{\delta^{m+1}}F(\eta) - \frac{Q}{r}\frac{1}{\delta^{m+1}}F(\eta)\right] = 0 \tag{18}$$

The equation of conservation of momentum, equation of energy, and equation of concentration are transformed to:

$$\begin{aligned}&\frac{(m+1)r^{m+1}}{\delta^{m+1}}\left(\frac{\rho_{nf}\delta^m}{\mu_0 r^{m-1}}\frac{\mathrm{d}\delta}{\mathrm{d}t}\right)F'(\eta) + c(n-1)c(n-2)\theta^{c(n-3)}F'(\eta)\\ &-\frac{2Q\rho_{nf}}{\mu_0}\frac{1}{\delta^{m+1}}F(\eta)F'(\eta) + c(n-1)\theta^{c(n-2)}\left[2F''(\eta) + 4F(\eta)\right]\\ &+\theta^{c(n-1)}\left[F'''(\eta) + 4F'(\eta)\right] - \frac{\sigma B_0^2 r^2}{\mu_0}F'(\eta) = 0\end{aligned} \tag{19}$$

$$\begin{aligned}&\left(\frac{k_{nf}}{\rho_{nf}C_p}\frac{\rho_{nf}}{\mu_0} + r\frac{16\sigma^*}{3k_{nf}\mu_0 C_p}T_\infty^3\right)\omega''(\eta) + \frac{(m+1)r^{m+1}}{\delta^{m+1}}\left(\frac{\rho_{nf}\delta^m}{\mu_0 r^{m-1}}\frac{\mathrm{d}\delta}{\mathrm{d}t}\right)\omega(\eta)\\ &+\frac{\theta^{c(n-1)}}{C_p}\frac{Q^2}{r^2\left(T_\infty - T_\omega\right)\delta^{m+1}}\left[4\left(F(\eta)\right)^2 + \left(F'(\eta)\right)^2\right]\\ &+\frac{\sigma B_0^2}{C_p\mu_0\left(T_\infty - T_\omega\right)\delta^{m+1}}Q^2\left(F(\eta)\right)^2 = 0\end{aligned} \tag{20}$$

$$\begin{aligned}&D_{nf}\frac{\rho_{nf}}{\mu_0}\phi''(\eta) + \frac{(m+1)r^{m+1}}{\delta^{m+1}}\left(\frac{\rho_{nf}\delta^m}{\mu_0 r^{m-1}}\frac{\mathrm{d}\delta}{\mathrm{d}t}\right)\phi(\eta)\\ &-\frac{k_r\rho_{nf}r^2}{\mu_0}\left[\phi(\eta) - \delta^{m+1}\right] + \frac{D_{nf}K_t}{T_\infty}\frac{\rho_{nf}r}{\mu_0}\frac{\left(T_\infty - T_\omega\right)}{\left(C_\infty - C_\omega\right)}\omega'(\eta) = 0\end{aligned} \tag{21}$$

where the observed non-dimensional parameters are:

Reynolds number: $Re = \frac{Q\rho_{nf}}{\mu_0}$, Hartmann number: $Ha = B_0 r\sqrt{\frac{\sigma}{\mu_0}}$, Unsteadiness Parameter: $\lambda = \frac{\rho_{nf}\delta^m}{\mu_0 r^{m-1}}\frac{\mathrm{d}\delta}{\mathrm{d}t}$, Prandtl number: $Pr = \frac{\mu_0}{\rho_{nf}\alpha}$ where $\alpha = \frac{k_{nf}}{\rho_{nf}C_p}$, Radiation parameter: $Rd = \frac{16\sigma^*}{3k_{nf}\mu_0 C_p}T_\infty^3$, Eckert number: $Ec = \frac{Q^2/r^2}{C_p\left(T_\infty - T_\omega\right)}$, Joule heating parameter: $J = \frac{\sigma B_0^2 Q^2}{C_p\mu_0\left(T_\infty - T_\omega\right)}$, Schmidt num-

ber: $Sc = \frac{\upsilon}{D_{nf}}$ where $\upsilon = \frac{\mu_0}{\rho_{nf}}$, Soret number: $Sr = \frac{D_{nf}K_t}{\upsilon T_\infty}\frac{T_\infty - T_\omega}{C_\infty - C_\omega}$, Chemical reaction parameter: $\Gamma = \frac{k_r \rho_{nf} r^2}{\mu_0}$.

Substituting the above dimensionless parameters into Equations (19)-(21) yielded:

$$\begin{aligned}&\frac{(m+1)r^{m+1}}{\delta^{m+1}}\lambda F'(\eta) + c(n-1)c(n-2)\theta^{c(n-3)}F'(\eta)\\&-2Re\frac{1}{\delta^{m+1}}F(\eta)F'(\eta) + c(n-1)\theta^{c(n-2)}\left[2F''(\eta)+4F(\eta)\right]\\&+\theta^{c(n-1)}\left[F'''(\eta)+4F'(\eta)\right] - Ha^2F'(\eta) = 0\end{aligned} \tag{22}$$

$$\begin{aligned}&\left(\frac{1}{Pr}+rRd\right)\omega''(\eta) + \frac{(m+1)r^{m+1}}{\delta^{m+1}}\lambda\omega(\eta)\\&+\frac{Ec}{\delta^{m+1}}\theta^{c(n-1)}\left[4\left(F(\eta)\right)^2+\left(F'(\eta)\right)^2\right] + \frac{J}{\delta^{m+1}}\left(F(\eta)\right)^2 = 0\end{aligned} \tag{23}$$

$$\frac{1}{Sc}\phi''(\eta) + \frac{(m+1)r^{m+1}}{\delta^{m+1}}\lambda\phi(\eta) - \Gamma\left[\phi(\theta)-\delta^{m+1}\right] + rS_r\omega'(\eta) = 0 \tag{24}$$

The transformed boundary conditions are:

At the center line, $\eta = 0$

$$F(0) = 1, F'(0) = 0, \omega(0) = \delta^{m+1}, \phi(0) = \delta^{m+1} \tag{25}$$

At the walls, $\eta = \alpha$

$$F'(\alpha) = -\gamma F(\alpha), \omega(\alpha) = 0, \phi(\alpha) = 0 \tag{26}$$

The Nusselt number, and Sherwood number for heat and mass transfer rates respectively are defined as:

$$Nu = -\sqrt{\frac{Re}{2-\epsilon}}\omega'(0) \tag{27}$$

$$Sh = -\sqrt{\frac{Re}{2-\epsilon}}\phi'(0) \tag{28}$$

where $\epsilon = \frac{2m}{m+1}$ is the wedge angle parameter.

2.3. Numerical Solution

In this study, the Spectral Collocation method is used to numerically solve the non-linear Ordinary Differential Equations (ODEs). This technique approximates solutions using a set of discrete points known as collocation points within a given domain. To get the numerical solutions, the higher-order non-linear ODEs are reduced to first-order ODEs by letting:

$$y_1 = F, y_2 = F', y_3 = F'', y_4 = \omega, y_5 = \omega', y_6 = \phi, y_7 = \phi' \tag{29}$$

The system of first-order equations is given by the matrix:

$$\begin{bmatrix} y_1' \\ y_2' \\ y_3' \\ y_4' \\ y_5' \\ y_6' \\ y_7' \end{bmatrix} = \begin{bmatrix} y_2 \\ y_3 \\ \dfrac{-(m+1)r^{m+1}}{\delta^{m+1}\theta^{c(n-1)}}\lambda y_2 - \dfrac{c(n-1)c(n-2)\theta^{c(n-3)}}{\theta^{c(n-1)}}y_2 + \dfrac{2Re}{\delta^{m+1}\theta^{c(n-1)}}y_1y_2 - \dfrac{c(n-1)\theta^{c(n-2)}}{\theta^{c(n-1)}}(2y_3+4y_1) + \dfrac{Ha^2}{\theta^{c(n-1)}}y_2 - 4y_2 \\ y_5 \\ \dfrac{1}{1+rRdPr}\left\{\dfrac{-Pr(m+1)r^{m+1}}{\delta^{m+1}}\lambda y_4 - \dfrac{PrEc}{\delta^{m+1}}\theta^{c(n-1)}\left(4y_1^2+y_2^2\right) - \dfrac{PrJ}{\delta^{m+1}}y_1^2\right\} \\ y_7 \\ Sc\left\{\dfrac{-(m+1)r^{m+1}}{\delta^{m+1}}\lambda y_5 + \Gamma\left(y_6 - \delta^{m+1}\right) - rSry_5\right\} \end{bmatrix}$$

Subject to the following reduced boundary conditions:

At the center line, $\eta = 0$

$$y_1(0)=1, y_2(0)=0, y_4(0)=\delta^{m+1}, y_6(0)=\delta^{m+1} \tag{30}$$

At the walls, $\eta = \alpha$

$$y_2(\alpha)=-\gamma y_1(\alpha), y_4(\alpha)=0, y_6(\alpha)=0 \tag{31}$$

3. Results and Discussions

This section displays the graphical results simulated and demonstrates how different flow parameters affect the velocity, temperature, and concentration profiles. The Nusselt and Sherwood numbers are tabulated. The Prandtl number is 6.2 due to the base fluid (water) used [4].

The effect of varying Reynolds number on the velocity profile is displayed in Figure 2. Varying the Reynolds number leads to an increment in the velocity of the nanofluid. Reynolds number is the ratio of inertia forces to viscous forces. Increasing the Reynolds number decreases the viscous forces thus fluid motion is less opposed resulting in an increase in the velocity of the nanofluid. The range of Reynolds number selected for this study was the range of $1 < Re < 2000$ was chosen to represent laminar and transitional flow regimes commonly encountered in microfluidic devices and is relevant to engineering applications such as heat exchangers and geothermal energy systems.

From Figure 3, augmenting the Hartmann number reduces the nanofluid velocity through the conduit. Increasing the Hartmann values increases the strength of the magnetic field, resulting in increased Lorentz force that opposes the motion of the nanofluid thus decreasing the velocity and hence leads to a suppression of convective heat transfer. The Hartmann number was varied from 0 to 50 to investigate the influence of the magnetic field on convective heat transfer.

The effect of varying the Eckert number on temperature profiles is displayed in Figure 4. Increasing the Eckert number consequently increases the temperature of the nanofluid. This is because the kinetic energy of nanoparticles increases making them more dynamic. This leads to the conversion of kinetic energy into heat energy thereby increasing the temperature of the nanofluid.

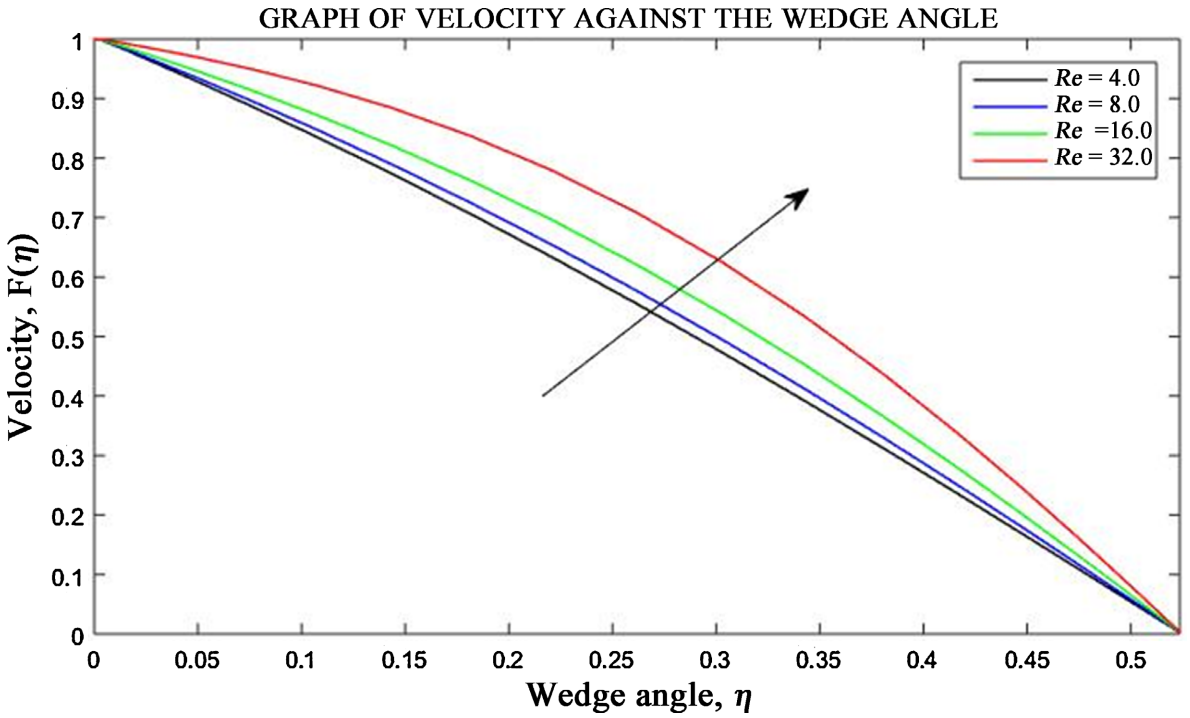

Figure 2. Effect of varying Reynolds number on velocity profile.

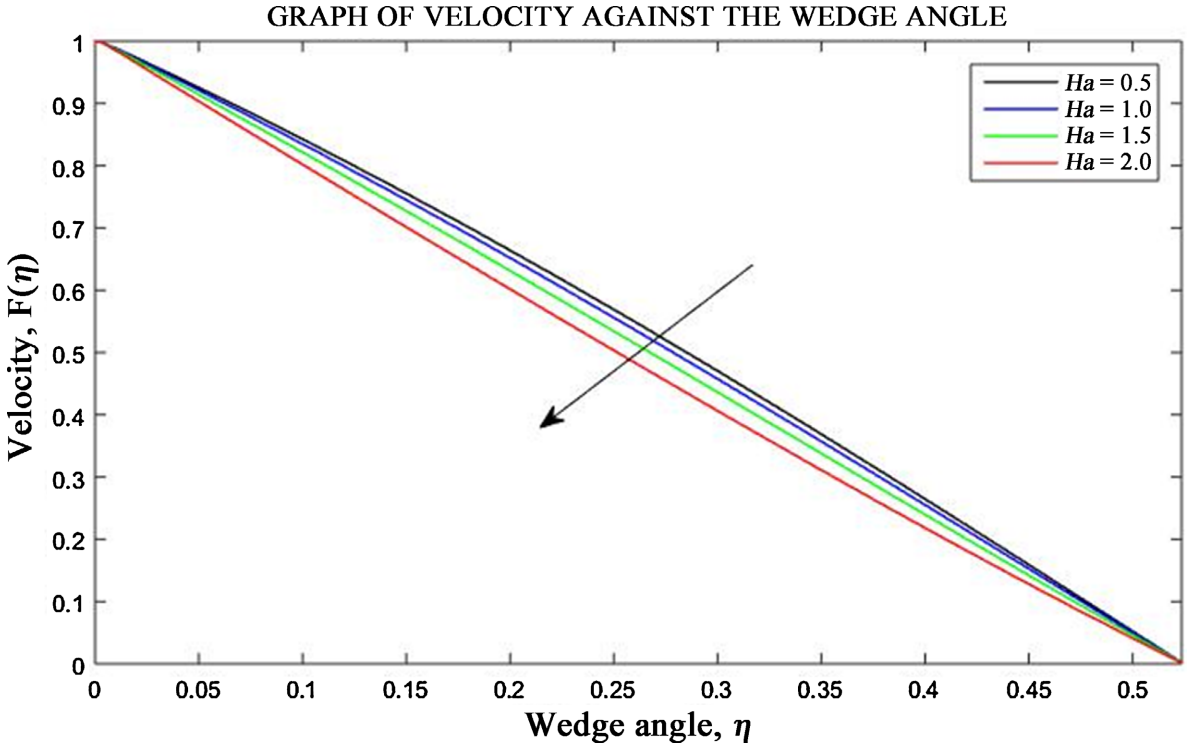

Figure 3. Effect of varying Hartmann number on velocity profile.

Figure 5 displays the effects of varying the Joule heating parameter. Increasing the Joule heating parameter augments the temperature of the nanofluid due to the flow having higher resistance to the flow of electric current leading to the conver-

sion of electrical energy into heat energy. The heat contributes to the internal energy resulting in a temperature rise.

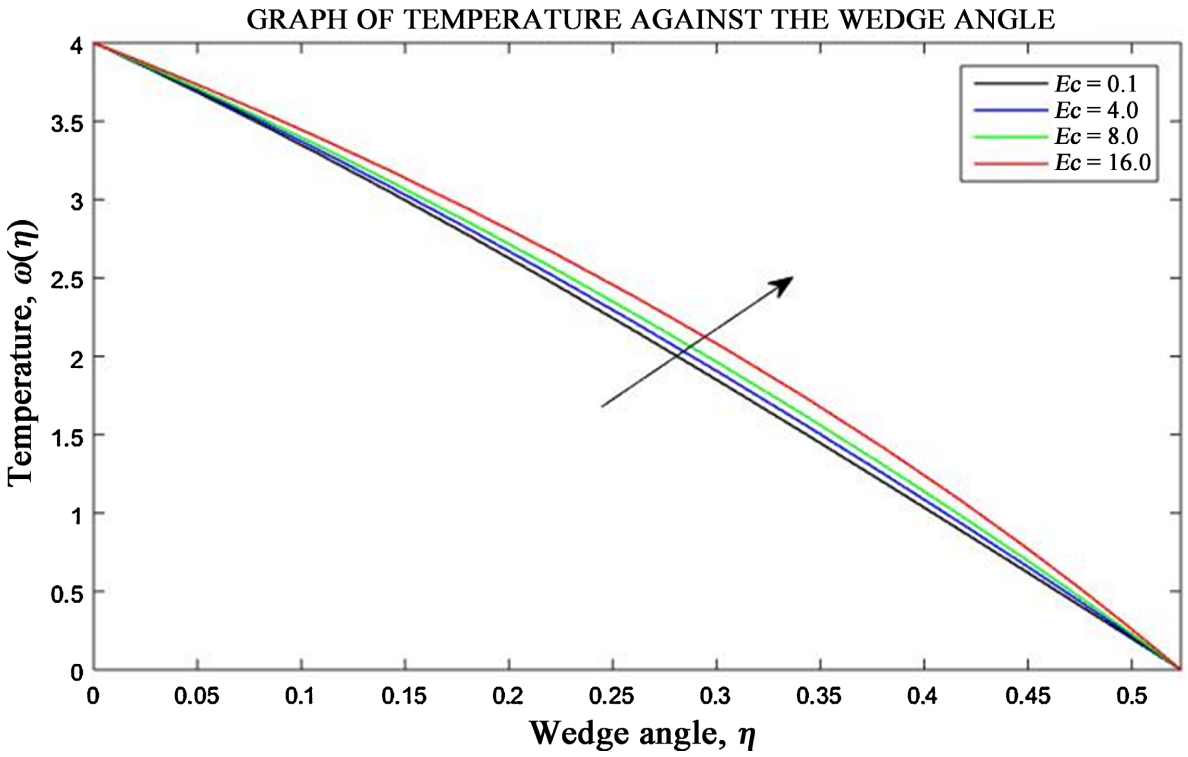

Figure 4. Effect of varying Eckert number on temperature profile.

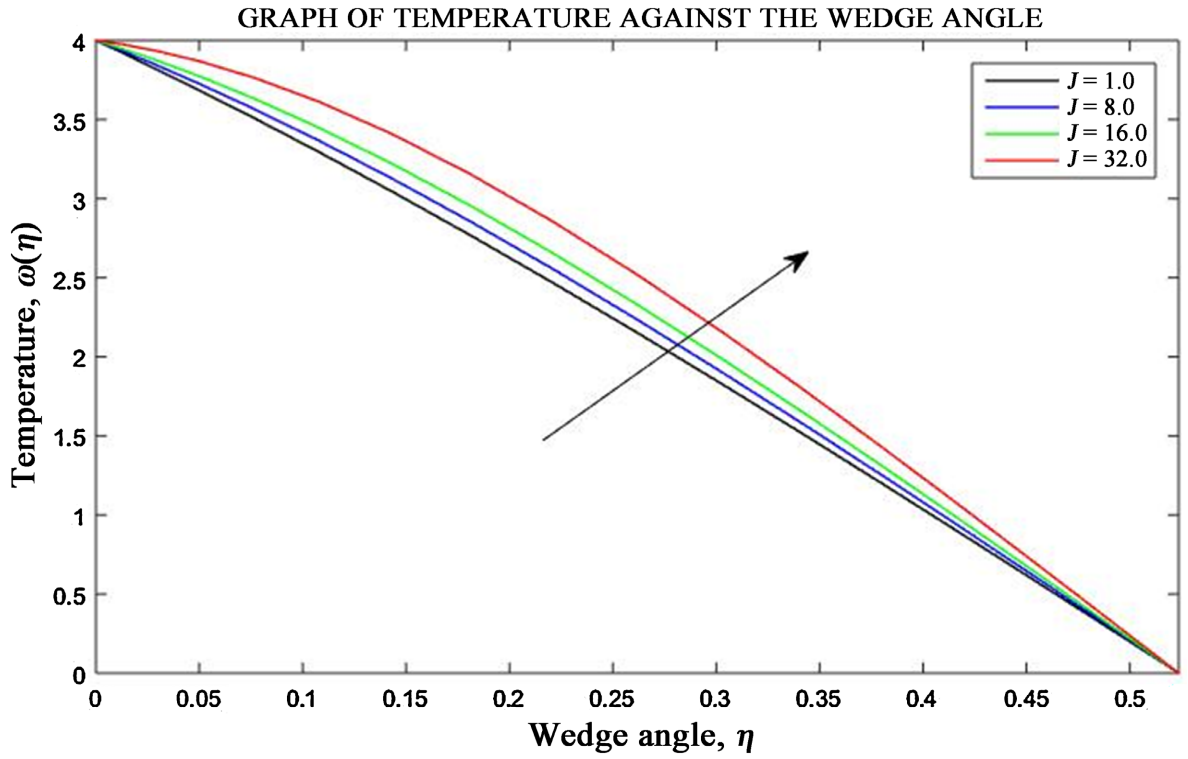

Figure 5. Effect of varying Joule heating parameter on temperature profile.

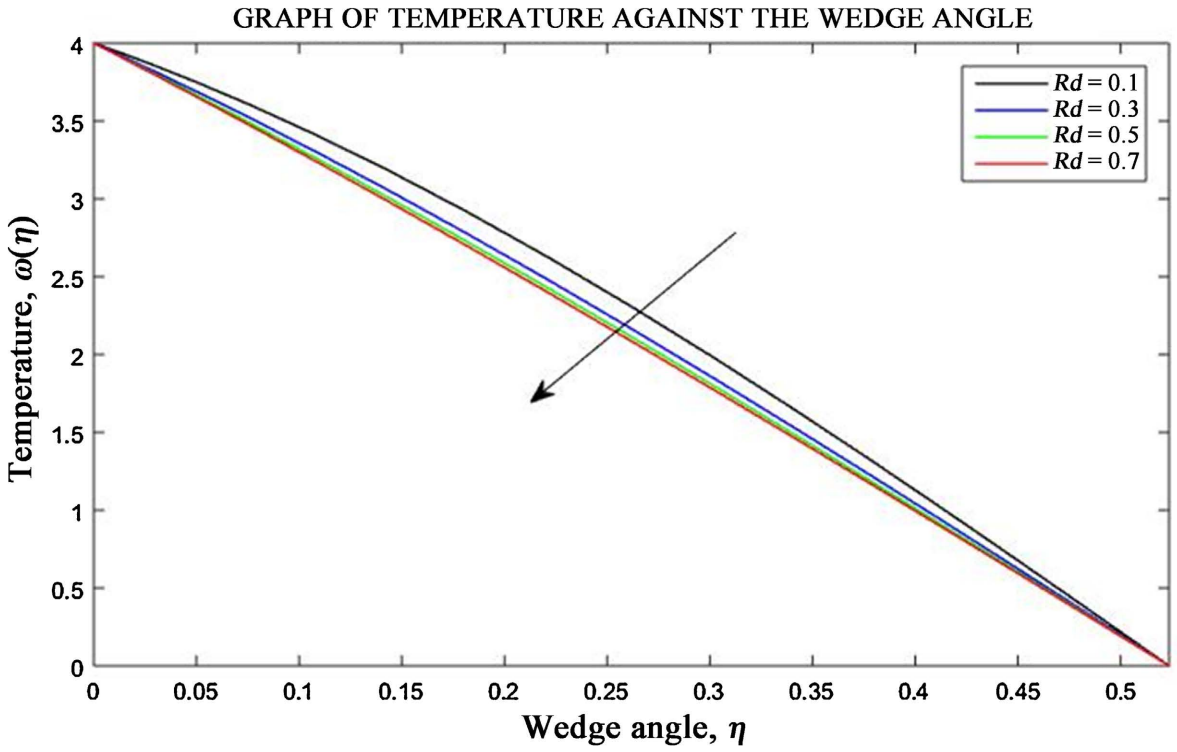

Figure 6. Effect of varying Radiation parameter on temperature profile.

The effect of radiation parameter on temperature profile is analyzed in **Figure 6**. The temperature of the nanofluid decreases when the radiation parameter is increased. This is because more heat is radiated out from a warmer surface to a cooler environment causing a cooling effect. Therefore, a net loss of thermal energy leads to a decrease in the overall temperature of the nanofluids. $Rd = 1$ corresponds to a moderate level of thermal radiation, while $Rd = 10$ explores the impact of strong radiation, relevant in high-temperature environments.

Figure 7 displays the effect of the unsteadiness parameter on the temperature of the nanofluid. Increasing the unsteadiness parameter increases the temperature of the nanofluid in the system. Varying the unsteadiness parameter means that the flow is unsteady with variations in time-dependent heat sources. This increases viscous dissipation which generates heat thus increasing the temperature.

Figure 8, portrays the effect of Schmidt number on the concentration profile. The concentration distribution decreases with an increase in the Schmidt number. Schmidt number is the ratio of momentum diffusivity (kinematic viscosity) to mass diffusivity. A higher Schmidt number implies that there is a decrease in mass diffusivity consequently decreasing the concentration of nanoparticles. The range of $0 < Sc < 100$ creates the comparison of mass transfer behavior of different fluids that is between gasses and liquids.

From **Figure 9**, the concentration of the nanofluid increases with an increase in the Soret number. Soret number is the ratio of thermal diffusion to mass diffusion. Increasing the parameter indicates that thermal diffusion is dominant. The temperature gradients result in migration of nanoparticles from regions of

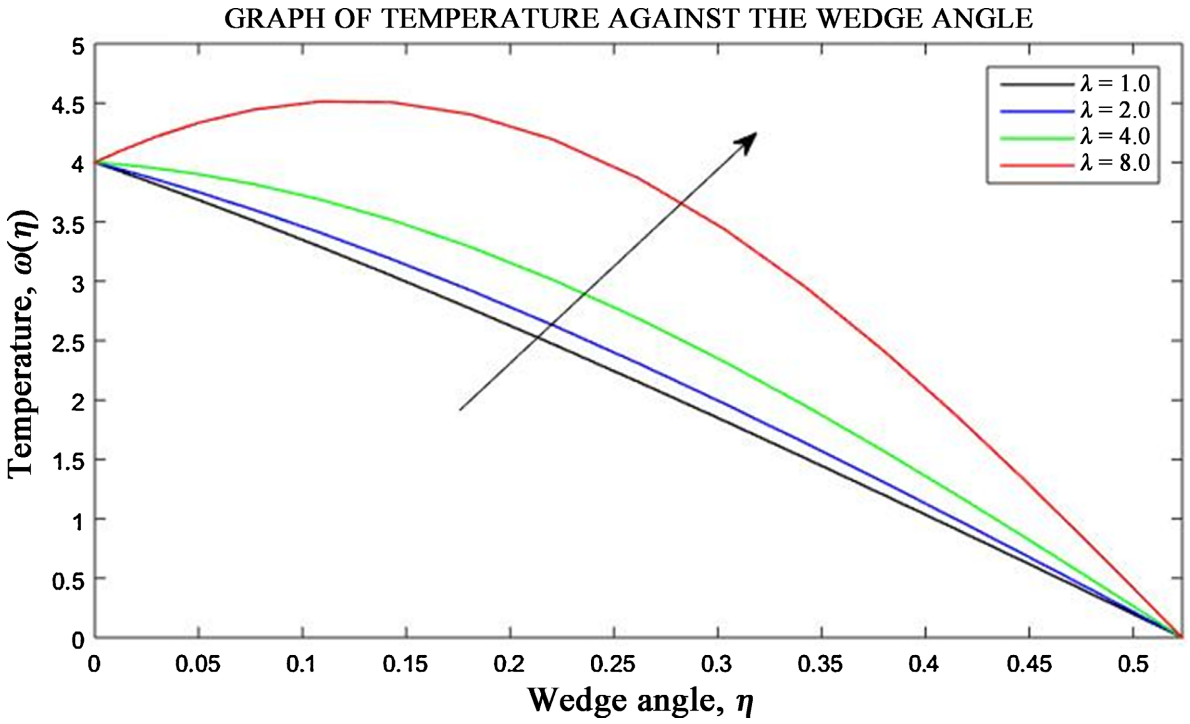

Figure 7. Effect of varying Unsteadiness parameter on temperature profile.

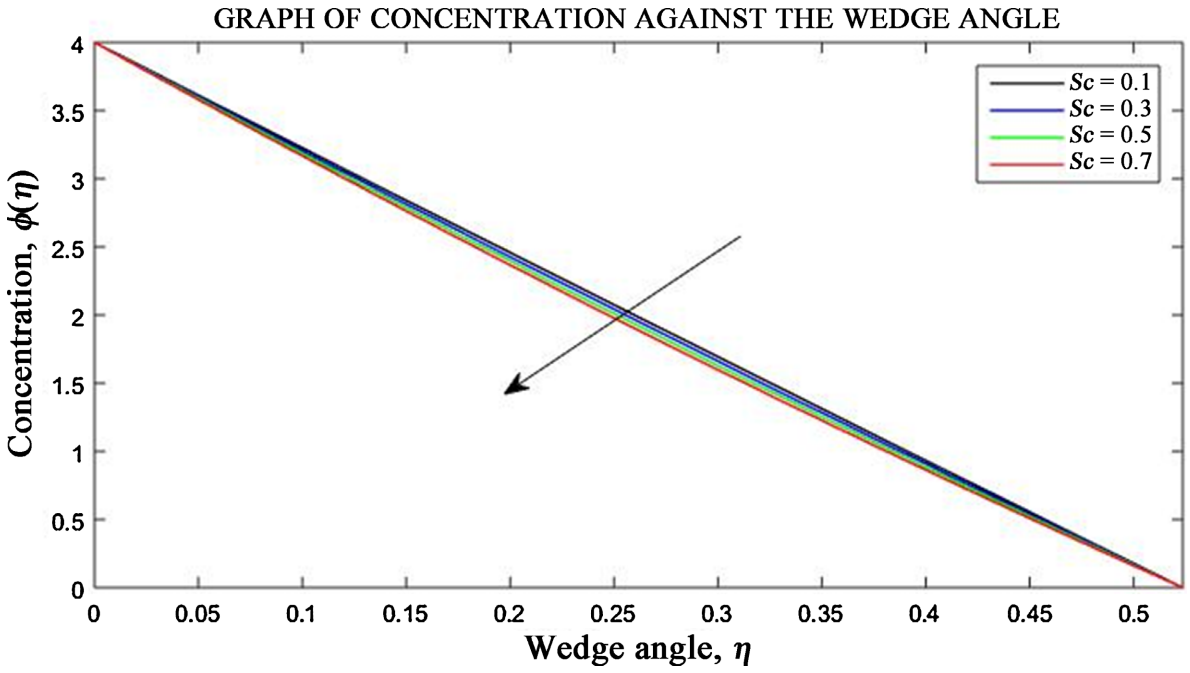

Figure 8. Effect of varying Schmidt number on concentration profile.

higher temperature to regions of lower temperature thus increasing the local concentration of nanoparticles in the nanofluid.

Figure 10 portrays the effect of Chemical reaction parameter on the concentration profile. As the Chemical reaction parameter is increased, the concentration also increases since the chemical reactions taking place within the nanofluid

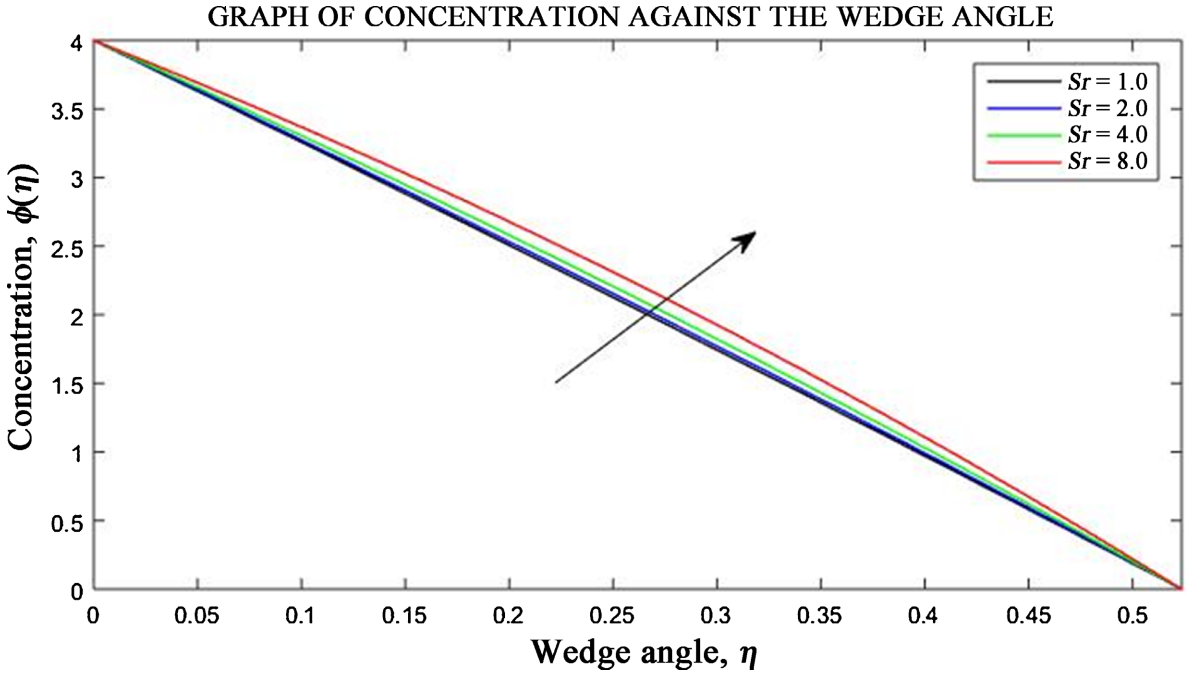

Figure 9. Effect of varying Soret number on concentration profile.

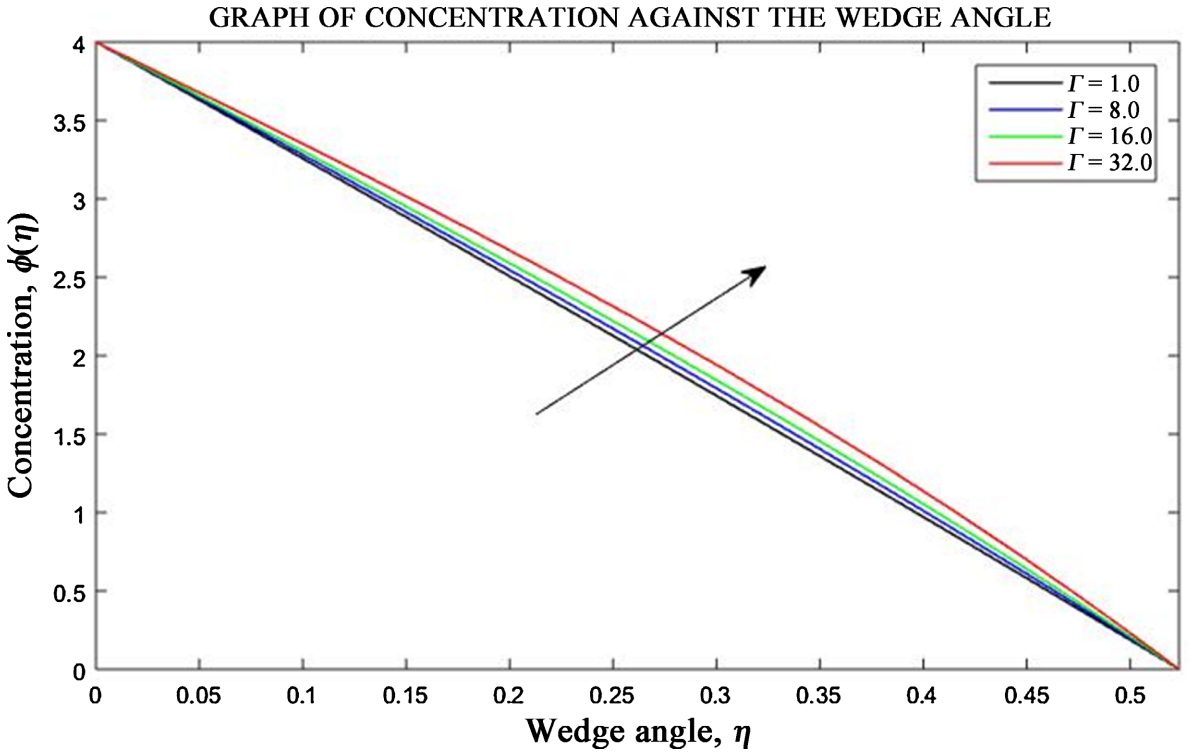

Figure 10. Effect of varying chemical reaction parameter on concentration profile.

become more rapid. Additional components are generated from the reactions which result in an increase of nanoparticles thus augmenting the concentration of the nanofluid.

3.1. Effects of Flow Parameters on Heat Transfer Rate

Numerical values for different physical parameters that affect the Nusselt number are displayed in Table 2. Increasing the Eckert number, Joule heating parameter, and unsteadiness parameter increases the rate of heat transfer whereas increasing the Radiation parameter decreases the rate of heat transfer. Increasing the Radiation parameter causes a cooling effect which reduces the overall temperature of the nanofluid. The rate of heat transfer is unaffected by variations in Schmidt number, Soret number, and Chemical reaction parameters.

Table 2. Results of heat transfer rate for different physical parameters.

Ec	*J*	λ	*Rd*	*Nu*
0.10	1.00	1.00	0.10	16.84203
0.00				18.18833
0.00				19.56915
0.00				22.33079
0.10	1.00	1.00	0.10	16.84203
	8.00			17.58512
	16.00			18.43437
	32.00			20.13286
0.10	1.00	1.00	0.10	16.84203
		2.00		18.46412
		4.00		22.45800
		8.00		35.45070
0.10	1.00	1.00	0.10	16.84203
			0.30	16.14026
			0.50	15.87334
			0.70	15.73271

3.2. Effects of Flow Parameters on Mass Transfer Rate

Table 3 displays the numerical simulations for different physical parameters on the Sherwood number. Increasing the Schmidt number, Soret number, unsteadiness parameter, and chemical reaction parameters increases the rate of mass transfer by augmenting the diffusion of nanoparticles within the nanofluid.

Table 3. Results of mass transfer rate for different physical parameters.

Sc	*Sr*	λ	Γ	*Sh*
0.10	1.00	1.00	1.00	15.87301
0.30				17.05739
0.50				18.23664
0.70				19.41080
0.10	1.00	1.00	1.00	15.87301
	2.00			16.29279

Continued

	4.00			17.13235
	8.00			18.81147
0.10	1.00	1.00	1.00	15.87301
		2.00		15.92925
		4.00		16.05042
		8.00		16.34905
0.10	1.00	1.00	1.00	15.87301
			8.00	16.82835
			16.00	17.89170
			32.00	19.93404

4. Validation of Results

The results are in agreement with the results obtained by habiyaremye *et al.* [4]. The temperature of the nanofluid increased with an increase in the Eckert number and the increase in the unsteadiness parameter led to an increase in the velocity for the nanofluid in the divergent section. The velocity of the nanofluid also increased with an increase in Reynold's number in the divergent section.

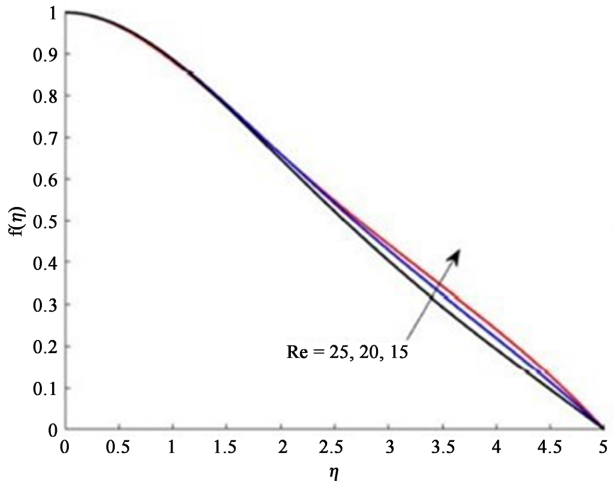

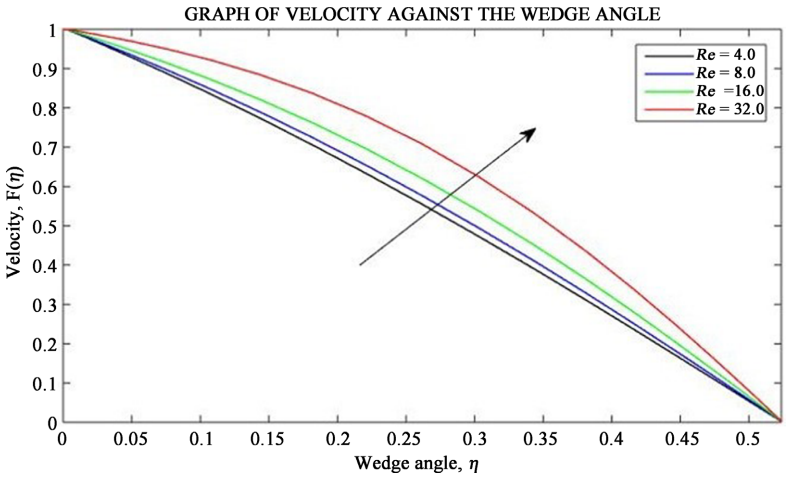

5. Conclusion

The rate of heat and mass transfer in unsteady MHD nanofluid flow through a divergent conduit with chemical reaction and radiation has been examined. The effects of dimensionless parameters on the flow variables, Nusselt number, and Sherwood number were investigated. From the findings, the following conclusions are deduced:

1) The fluid flow velocity was enhanced with an increase in Reynolds number and Hartmann number.

2) The temperature profiles increased when the Eckert number, Joule heating parameter, and unsteadiness parameter increased, whereas increasing the radiation parameter decreased the temperature of the nanofluid.

3) Higher values of the Soret number, chemical reaction parameter, and unsteadiness parameter led to an increase in the concentration profile while increasing the Schmidt number reduced the concentration profile.

4) The rate of heat transfer increased by increasing the Eckert number, Joule heating parameter, and unsteadiness parameter while it decreased when the radiation parameter was increased.

5) The rate of mass transfer increased with an increase in the Schmidt number, Soret number, unsteadiness parameter, and Chemical reaction parameter.

6. Recommendations

Heat and mass transfer in MHD nanofluid flows is a wide area of research. Further research to consider include:

- Influence of variable magnetic field on heat and mass transfer in unsteady MHD nanofluid flow through a divergent conduit with chemical reaction and radiation.
- Effect of strong magnetic field on heat and mass transfer in unsteady MHD nanofluid flow through a divergent conduit with chemical reaction and radiation.
- Heat and mass transfer on unsteady MHD nanofluid of compressible flow through a divergent conduit with chemical reaction and radiation.

Data Availability

The data used to support the study's findings are accessible from the corresponding author upon request.

Acknowledgements

The authors express their gratitude to Jomo Kenyatta University of Agriculture and Technology for their support and to the anonymous reviewers for their valuable comments.

Conflicts of Interest

The authors declare no conflicts of interest regarding the publication of this paper.

References

[1] Haroun, N.A., Sibanda, P., Mondal, S. and Motsa, S.S. (2015) On Unsteady MHD Mixed Convection in a Nanofluid Due to a Stretching/shrinking Surface with Suction/Injection Using the Spectral Relaxation Method. *Boundary Value Problems*, **2015**, Article No. 24. https://doi.org/10.1186/s13661-015-0289-5

[2] Phelan, P.E., Bhattacharya, P. and Prasher, R.S. (2005) Nanofluids for Heat Transfer Applications. *Annual Review of Heat Transfer*, **14**, 255-275. https://doi.org/10.1615/annualrevheattransfer.v14.160

[3] Alfvén, H. (1942) Existence of Electromagnetic-Hydrodynamic Waves. *Nature*, **150**, 405-406. https://doi.org/10.1038/150405d0

[4] Habiyaremye, F., Wainaina, M. and Kimathi, M. (2022) The Effect of Heat and Mass Transfer on Unsteady MHD Nanofluid Flow through Convergent-Divergent Channel. *International Journal of Fluid Mechanics & Thermal Sciences*, **8**, 10-22. https://doi.org/10.11648/j.ijfmts.20220801.12

[5] Zubair Akbar, M., Ashraf, M., Farooq Iqbal, M. and Ali, K. (2016) Heat and Mass Transfer Analysis of Unsteady MHD Nanofluid Flow through a Channel with Moving Porous Walls and Medium. *AIP Advances*, **6**, Article No. 045222. https://doi.org/10.1063/1.4945440

[6] Govardhan, K., Narender, G. and Sarma, G.S. (2020) Heat and Mass Transfer in MHD Nanofluid over a Stretching Surface along with Viscous Dissipation Effect. *International Journal of Mathematical, Engineering and Management Sciences*, **5**, 343-352. https://doi.org/10.33889/ijmems.2020.5.2.028

[7] Ullah, I., Khan, I. and Shafie, S. (2016) MHD Natural Convection Flow of Casson Nanofluid over Nonlinearly Stretching Sheet through Porous Medium with Chemical Reaction and Thermal Radiation. *Nanoscale Research Letters*, **11**, 1-15. https://doi.org/10.1186/s11671-016-1745-6

[8] Pushpalath, K., Sugunamma, V., Reddy, J.V.R. and Sandeep, N. (2016) Heat and Mass Transfer in Unsteady MHD Casson Fluid Flow with Convective Boundary Conditions. *International Journal of Advanced Science and Technology*, **91**, 19-38. https://doi.org/10.14257/ijast.2016.91.03

[9] Sujatha, T., Reddy, K.J. and Kumar, J.G. (2019) Chemical Reaction Effect on Nonlinear Radiative MHD Nanofluid Flow over Cone and Wedge. *Defect and Diffusion Forum*, **393**, 83-102. https://doi.org/10.4028/www.scientific.net/ddf.393.83

[10] Richard Onyango, E., Ngugi Kinyanjui, M., Kimathi, M. and Mohan Uppal, S. (2020) Heat and Mass Transfer on MHD Jeffrey-Hamel Flow in Presence of Inclined Magnetic Field. *Applied and Computational Mathematics*, **9**, 108-117. https://doi.org/10.11648/j.acm.20200904.11

[11] Mohyud-Din, S.T., Khan, U., Ahmed, N. and Rashidi, M.M. (2018) A Study of Heat and Mass Transfer on Magnetohydrodynamic (MHD) Flow of Nanoparticles. *Propulsion and Power Research*, **7**, 72-77. https://doi.org/10.1016/j.jppr.2018.02.001

[12] Nyariki, E.M., Kinyanjui, M.N. and Abonyo, J.O. (2023) Heat and Mass Transfers in a Two-Phase Stratified Turbulent Fluid Flow in a Geothermal Pipe with Chemical Reaction. *Journal of Applied Mathematics and Physics*, **11**, 484-513. https://doi.org/10.4236/jamp.2023.112030

[13] Nyabuti, V., Kiogora, P.R., Onyango, E. and Nyawade, E. (2024) Unsteady MHD Nanofluid Flow through a Divergent Conduit with Chemical Reaction and Radiation. *International Journal of Fluid Mechanics & Thermal Sciences*, **10**, 1-14. https://doi.org/10.11648/j.ijfmts.20241001.11

[14] Sharma, K., Vijay, N., Mabood, F. and Badruddin, I.A. (2022) Numerical Simulation of Heat and Mass Transfer in Magnetic Nanofluid Flow by a Rotating Disk with Variable Fluid Properties. *International Communications in Heat and Mass Transfer*, **133**, Article ID: 105977. https://doi.org/10.1016/j.icheatmasstransfer.2022.105977

[15] A. Reddy, P.S. and Chamkha, A. (2018) Heat and Mass Transfer Characteristics of MHD Three-Dimensional Flow over a Stretching Sheet Filled with Water-Based Alumina Nanofluid. *International Journal of Numerical Methods for Heat & Fluid Flow*, **28**, 532-546. https://doi.org/10.1108/hff-02-2017-0061

[16] Pantokratoras, A. (2014) Natural Convection along a Vertical Isothermal Plate with Linear and Non-Linear Rosseland Thermal Radiation. *International Journal of Thermal Sciences*, **84**, 151-157. https://doi.org/10.1016/j.ijthermalsci.2014.05.015

[17] Dogonchi, A.S. and Ganji, D.D. (2016) Investigation of MHD Nanofluid Flow and Heat Transfer in a Stretching/shrinking Convergent/divergent Channel Considering Thermal Radiation. *Journal of Molecular Liquids*, **220**, 592-603. https://doi.org/10.1016/j.molliq.2016.05.022

[18] Mahbubul, I.M., Fadhilah, S.A., Saidur, R., Leong, K.Y. and Amalina, M.A. (2013) Thermophysical Properties and Heat Transfer Performance of Al_2O_3/r-134a Nanorefrigerants. *International Journal of Heat and Mass Transfer*, **57**, 100-108. https://doi.org/10.1016/j.ijheatmasstransfer.2012.10.007

[19] Syam Sundar, L., Singh, M.K. and Sousa, A.C.M. (2013) Investigation of Thermal Conductivity and Viscosity of Fe3o4 Nanofluid for Heat Transfer Applications. *International Communications in Heat and Mass Transfer*, **44**, 7-14. https://doi.org/10.1016/j.icheatmasstransfer.2013.02.014

[20] Nagler, J. (2017) Jeffery-Hamel Flow of Non-Newtonian Fluid with Nonlinear Viscosity and Wall Friction. *Applied Mathematics and Mechanics*, **38**, 815-830. https://doi.org/10.1007/s10483-017-2206-8

[21] Sattar, M.A. (2013) Derivation of the Similarity Equation of the 2D Unsteady Boundary Layer Equations and the Corresponding Similarity Conditions. *American Journal of Fluid Dynamics*, **3**, 135.

Abbreviations

PDE	Partial differential equations
ODE	Ordinary differential equations
MHD	Magneto-hydrodynamics
MATLAB	Matrix Laboratory

Nomenclature

Symbol	Meaning	SI Units
C_p	Specific heat capacity	$J \cdot kg^{-1} \cdot K^{-1}$
u, v, w	velocity components	$m \cdot s^{-1}$
t	Time	s
P	Pressure	N/m^2
T	Temperature of the fluid	K
C	Concentration of the fluid	kg/m^3
K	Thermal conductivity	W/(mK)
F	Body Forces	N
D_{nf}	Mass diffusivity of nanoparticles	m^2/s
B_0	Strength of Magnetic Field	
q_{rad}	Radiative heat flux	
Re	Reynolds number	
Pr	Prandtl	
Ha	Hartmann number	
Sc	Schmidt number	
Rd	Radiation parameter	
C_f	Skin friction coefficient	
Nu	Nusselt number	
Sh	Sherwood number	
r, θ, z	Cylindrical coordinate system	
∇	Gradient Operator	$\left(\frac{\hat{r}}{r}\frac{\partial}{\partial r}(r)+\frac{\hat{\theta}}{r}\frac{\partial}{\partial \theta}+\hat{z}\frac{\partial}{\partial z}\right)$